

Cross-correlating dark sirens and galaxies: measurement of H_0 from GWTC-3 of LIGO-Virgo-KAGRA

Suvodip Mukherjee,^{1,*} Alex Krolewski,^{2,1,†} Benjamin D. Wandelt,^{3,4,‡} and Joseph Silk^{3,5,6,§}

¹*Perimeter Institute for Theoretical Physics, 31 Caroline St. North, Waterloo, ON N2L 2Y5, Canada*

²*AMTD Fellow, Waterloo Centre for Astrophysics,
University of Waterloo, Waterloo ON N2L 3G1, Canada*

³*Institut d'Astrophysique de Paris, UMR 7095, CNRS,
Sorbonne Université, 98bis Boulevard Arago, 75014 Paris, France*

⁴*Center for Computational Astrophysics, Flatiron Institute, 162 5th Avenue, 10010, New York, NY, USA*

⁵*Beecroft Institute for Cosmology and Particle Astrophysics,
University of Oxford, Keble Road, Oxford OX1 3RH, UK*

⁶*The Johns Hopkins University, Department of Physics & Astronomy,
Bloomberg Center for Physics and Astronomy, Room 366,
3400 N. Charles Street, Baltimore, MD 21218, USA*

(Dated: March 9, 2022)

We measure the Hubble constant of the Universe using spatial cross-correlation between gravitational wave (GW) sources without electromagnetic counterparts from the third GW Transient Catalog (GWTC-3), and the photometric galaxy surveys 2MPZ and WISE-SuperCOSMOS. Using the eight well-localised GW events, we obtain Hubble constant $H_0 = 68.2^{+26.0}_{-6.2}$ km/s/Mpc (median and 68.3% equal-tailed interval (ETI)) after marginalizing over the matter density and the GW bias parameters. Though the constraints are weak due to a limited number of GW sources and poor sky localization, they are not subject to assumptions regarding the GW mass distribution. By combining this measurement with the Hubble constant measurement from binary neutron star GW170817, we find a value of Hubble constant $H_0 = 67.0^{+6.3}_{-3.8}$ km/s/Mpc (median and 68.3% ETI).

Introduction – Discovery of gravitational waves (GW) [1] by the LIGO-Virgo-KAGRA (LVK) collaboration [2–7] has opened a new observational window to study the cosmos using transient sources such as binary neutron stars (BNSs), binary black holes (BBHs) and neutron star black holes (NSBHs). GW sources are uniquely accurate tracers of the luminosity distance. They can therefore be used to measure the expansion history of the Universe (Schutz [8]). This fact has earned GW sources the name *standard sirens*. However, one of the key ingredients required to measure the expansion history using GW sources is an independent measurement (or inference) of the GW source redshifts. In the absence of electromagnetic counterparts, a promising way to infer the GW source redshifts is through spatial cross-correlation of the GW sources with galaxies. By using the clustering redshift of the GW sources [9–11] or a 3D-cross correlation generalizing the Alcock-Paczynski effect [12–16], we can measure the cosmic expansion history after marginalizing over the GW bias parameters. Apart from cross-correlation techniques, statistical host identification [8, 17–26] and GW mass distribution [27–34] can also be used to infer redshifts for BBHs. However, the mass distribution of the BBHs can have intrinsic redshift dependence that influences parameter estimation, if the full mass distribution gets affected [32, 34].

LVK dark standard sirens have been used to measure the expansion history using O1+O2 data [23] and O1+O2+O3 data [35], in tandem with GLADE [36] and GLADE+ [37] for statistical host identification. The latest LVK measurement yields $H_0 = 68^{+8}_{-6}$ km/s/Mpc (68.3%

highest density interval (HDI)) after combining with the bright siren GW170817 [35]. Other independent measurements of H_0 using statistical host identification have also been performed on the GW data [38, 39].

In this paper, we make the first measurement of the Hubble constant H_0 using the cross-correlation between the GWTC-3 catalog of the LVK collaboration [40] and the photometric galaxy surveys 2MPZ [41] and WISE-SuperCOSMOS (WSC) [42].¹ Though currently we cannot detect clustering between GW sources and galaxies due to the limited number of GW sources and poor sky localization error, this is the first proof of principle of this technique on data. The current measurement is limited by the lack of high redshift galaxies and the number of well localised GW sources. The statistical power in the cross-correlation technique with limited number of sources having poor sky localization error will be similar to (but not worse than) the statistical host identification technique. However, the cross-correlation measurement does not depend on assumptions about the GW source population, and provides an independent technique to infer the value of the Hubble constant.

Method – The compact objects of both astrophysical and primordial origin will exhibit spatial correlation with galaxies due to the underlying distribution of dark matter. This spatial correlation can be used to infer the clustering redshift of the dark standard sirens, by cross-correlating with photometric (or spectroscopic) galaxy

¹ We have not used DeCALs [43] in this analysis, as discussed later

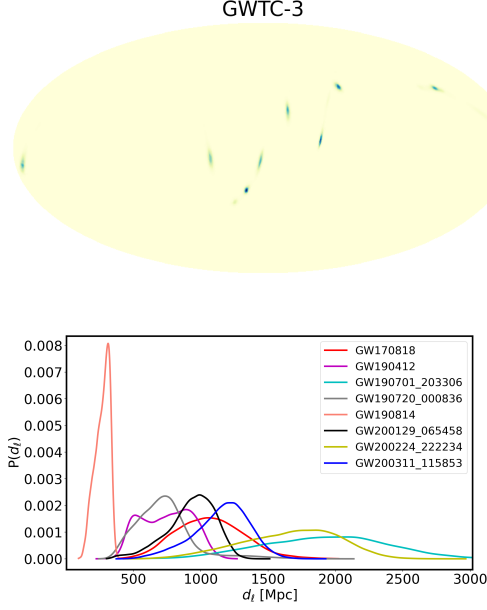


FIG. 1: The sky map in equatorial coordinates (top) and the luminosity distance (below) of the eight selected GW sources from GWTC-3.

samples, as shown in [12, 14, 15]. The clustering redshift technique is also used widely in other cosmological studies [44–46]. From the observed spatial distribution of GW sources (or galaxies) $n_X(\theta, \phi)$, we can construct a density map as $\delta^X(\theta, \phi) = \frac{n_X(\theta, \phi)}{\bar{n}_X} - 1$ (where \bar{n}_X is the mean density and $X \in \{\text{GW}, \text{g}\}$). The angular correlation between a galaxy map and a GW map in the spherical harmonic basis² ($\delta^X(\theta, \phi) = \sum_{\ell m} \delta_{\ell m}^X Y_{\ell m}(\theta, \phi)$) can be written as $\hat{C}_\ell^{XY} = \frac{\sum_m \delta_{\ell m}^X \delta_{\ell m}^{*Y}}{2\ell+1}$. \hat{C}_ℓ^{XY} denotes the pseudo auto (for $X = Y$) and cross (for $X \neq Y$) angular power spectrum obtained from the masked density maps, denoted by $\hat{\delta}$. One can construct the binned average power spectrum as $\hat{C}_{\ell_b}^{XY} = \sum_{\ell \in \ell_b} W_\ell C_\ell^{XY}$, where W_ℓ denotes the normalised window function. The corresponding covariance matrix for the angular power spectrum in the Gaussian limit can be written as

$$\Sigma_{C_\ell^{XY} C_{\ell'}^{XY}} = \delta_{\ell\ell'} \frac{(C_\ell^{XX} + n_\ell^X)(C_\ell^{YY} + n_\ell^Y) + C_\ell^{XY}}{(2\ell+1)f_{\text{sky}}\Delta\ell}, \quad (1)$$

where n_ℓ^X denotes the shot noise for tracer X , equal to the inverse of its number density. For the cross power spectrum, the shot noise is zero. $f_{\text{sky}} \equiv \Omega_s/4\pi$ denotes the overlapping sky fraction between GW sources and galaxy catalog, and $\Delta\ell$ denotes the bin width in ℓ -space over which we estimate the band-averaged power spectrum. Choosing a large bin width makes it possible to reduce the correlation between different multipoles.

We estimate the cosmological parameters, Hubble constant H_0 and matter density Ω_m , along with the GW bias parameter $b_{GW}(z) = b_{GW}(1+z)^\alpha$ using a Bayesian framework.³ The posterior on the parameters given the GW data $\mathbf{\vartheta}_{GW}$ with N_{GW} sources and galaxy data \mathbf{d}_g with photometric redshifts z_c can be written, after marginalizing over the nuisance parameters $\Theta_n \in \{b_{GW}, \alpha\}$, as [14, 16]

$$\begin{aligned} \mathcal{P}(\Theta_c | \mathbf{\vartheta}_{GW}, \mathbf{d}_g, z_c) &\propto \iint d\Theta_n dz \prod_{i=1}^{N_{GW}} \Pi(z) \Pi(\Theta_n) \Pi(\Theta_c) \\ &\times \mathcal{P}(\mathbf{\vartheta}_{GW} | \{C_\ell^{gg}(z_c)\}, \Theta_n, \mathbf{d}_g(z_c)) \\ &\times \mathcal{P}(\mathbf{d}_g(z_c) | \{C_\ell^{gg}(z_c)\}) \mathcal{P}(z|z_c) \\ &\times \mathcal{P}(\{d_\ell^i\}_{GW} | z, \Theta_c, \{\hat{\theta}^i, \hat{\phi}^i\}_{GW}), \end{aligned} \quad (2)$$

where the likelihood $\mathcal{P}(\mathbf{\vartheta}_{GW} | \{C_\ell^{gg}(z_c)\}, \Theta_n, \mathbf{d}_g(z_c))$ is written as

$$\begin{aligned} \mathcal{P}(\mathbf{\vartheta}_{GW} | \{C_\ell^{gg}(z_c)\}, \Theta_n, \mathbf{d}_g(z_c)) &\propto \\ \exp\left(-0.5 \sum_{\ell_b, \ell'_b}^{\ell_{\max}} D(\ell_b, z_c) \Sigma_{C_{\ell_b}^{XY} C_{\ell'_b}^{XY}}^{-1} D(\ell'_b, z_c)\right), \end{aligned} \quad (3)$$

Here, ℓ_{\max} denotes the maximum value of the multipoles that can be explored (which depends on the sky localization error) and $D(\ell, z_c) = \hat{C}_\ell^{GWg}(z_c) - C_\ell^{GWg}(z_c)$. The angular cross-correlation power spectrum $\hat{C}_\ell^{GWg}(z_c)$ is obtained from cross-correlating GW sources detected above a network matched filtering SNR with galaxy catalogs $\mathbf{d}_g(z_c)$. The theoretical angular cross-power spectrum is written in terms of the galaxy auto-power spectrum $C_\ell^{gg}(z_c)$, the galaxy bias $b_g(z_c)$ and GW bias $b_{GW}(z_c)$ as $C_\ell^{GWg}(z_c) = b_{GW}(z_c)/b_g(z_c) C_\ell^{gg}(z_c)$. The term $\mathcal{P}(\mathbf{d}_g(z_c) | \{C_\ell^{gg}(z_c)\})$ denotes the galaxy density field given the auto-power spectrum $C_\ell^{gg}(z_c)$, and $\mathcal{P}(z|z_c)$ is the probability distribution of true redshifts within z_c , capturing the photometric redshift error on the galaxies. The likelihood on the luminosity distance given the cosmological parameters Θ_c and redshift is denoted by $\mathcal{P}(\{d_\ell^i\}_{GW} | z, \Theta_c, \{\hat{\theta}^i, \hat{\phi}^i\}_{GW})$, and the prior on the redshift, cosmological parameters, and nuisance parameters are denoted by $\Pi(z)$, $\Pi(\Theta_c)$, and $\Pi(\Theta_n)$ respectively.

GW catalog and selection function : In this analysis, we use the publicly available GW catalog GWTC-3 detected by the LVK collaboration [40]. As the most constraining estimations of cosmological parameters can be made from sources with high matched filtering SNR, we select samples from GWTC-3 with $\text{SNR} \geq 11$. Also,

³ [14, 16] give a detailed derivation of the Bayesian framework. The framework is written for a spectroscopic redshift survey, so an additional term to include to error on the redshift is included.

² $Y_{\ell m}(\theta, \phi)$ denote the spherical harmonic basis.

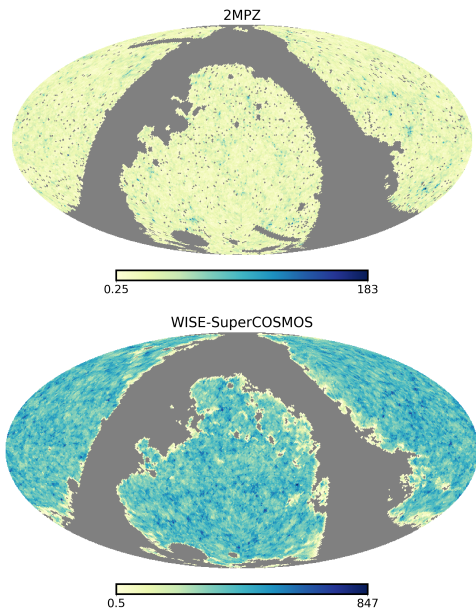


FIG. 2: The sky map along with mask (gray) in equatorial coordinates of 2MPZ (top) and WSC (bottom).

as the cross-correlation technique is most effective for sources with better sky localization error, we further select sources with sky localization error $\Delta\Omega \leq 30$ sq. deg at 68.3% CI. These two selections lead to a total of eight GW events, namely GW170818, GW190412, GW190814, GW190701.203306, GW190720.000836, GW200129.0065458, GW200224.222234, and GW200311.115853. The posteriors on the sky position and the luminosity distance are shown in Fig. 1.

Galaxy catalog and selection function: We use galaxies from the 2MASS Photometric Redshift catalog [2MPZ, Fig. 2; 41] and WISE cross SuperCOSMOS Photometric Redshift catalog [WSC, Fig. 2; 42].⁴ 2MPZ is derived from the all-sky 2MASS near-infrared extended source catalog (XSC) [47, 48], cross-matched to the infrared AllWISE [49] and optical SuperCOSMOS catalogs [50–53]. WSC is constructed in a similar way, but cross-matching AllWISE and SuperCOSMOS only. For WSC, we further apply a color cut of $W1 - W2 > 0.2$ to the publicly available sample to reduce stellar contamination and increase uniformity [54]. The galaxy samples are further described and validated in [55], including the impact of changing the selection criteria.

The choice of mask⁵ for the 2MPZ [41] and WSC [42] galaxy surveys left nearly 65% of the sky. At higher redshift (and with lower stellar contamination than WSC), DeCALs [43] covers about 50% of the sky area. Although

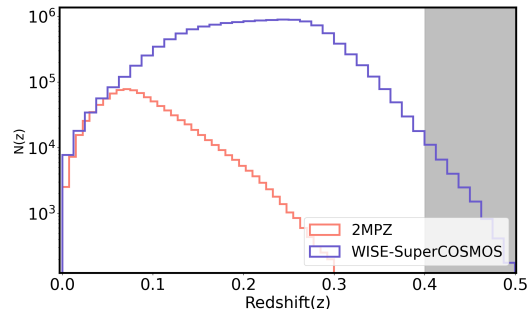


FIG. 3: The redshift distribution of the 2MPZ (in orange) and WSC (in blue) galaxies. The shaded region shows the redshift range that is shot noise dominated.

the sky fraction reduction is modest for DeCALs, it unfortunately misses four out of the eight GW events. As a result, we use only 2MPZ and WSC in this paper.

The redshift distributions of 2MPZ and WSC are shown in Fig. 3 in orange and blue respectively. At $z < 0.1$ we use 2MPZ despite its lower number density, as it has more precise photometric redshifts and far less stellar contamination. For $z > 0.1$, we use WSC exclusively. At $0.3 < z < 0.4$, WSC clustering is shot noise dominated at $\ell > 60$, and is shot noise dominated at all ℓ for $z > 0.4$. We still measure galaxy clustering at $0.4 < z < 0.5$, albeit with increased errors (total SNR ~ 4.7 , after subtracting shot noise, over the relevant scales $10 < \ell < 40$), but exclude $z > 0.5$ where there are very few WSC galaxies. For both surveys, photometric redshifts are trained using the ANNz algorithm [56], yielding typical redshift errors $\sigma_z = 0.015$ for 2MPZ and $\sigma_z/(1+z) = 0.033$ for WSC.

Results – We have adopted the following uniform prior ranges: $\Pi(H_0) = \mathcal{U}[20, 120]$ km/s/Mpc, $\Pi(\Omega_m) = \mathcal{U}[0.1, 0.4]$, $\Pi(b_{GW}) = \mathcal{U}[0.1, 6]$, and $\Pi(\alpha) = \mathcal{U}[-2, 2]$. We use a redshift bin-width of $\Delta z = 0.1$ which is nearly three times the WSC photo- z error. For the cross-correlation we include only the lower multipoles $\ell \leq 30$ and consider different choices of bins $\Delta\ell = 5, 10, 15$ in the analysis. We do not use the first ℓ -bin in the analysis to minimize low- ℓ contaminations.

From the auto-power spectrum, we infer the galaxy bias $b_g(z)$ by fitting a simple linear bias times the non-linear “Halofit” matter power spectrum model [57]. We use the NaMaster code [58, 59] to measure pseudo- C_ℓ for each redshift slice, applying a 1° apodization [“ C^1 apodization”; 60] to the galaxy mask. For WSC, we additionally deproject the Schlegel-Finkbeiner-Davis [61] dust extinction map and a stellar density map from Gaia [62] to reduce the impact of contamination, following [63]. We fit the one-parameter bias model to the data in the range $10 < \ell < 40$, with shot noise fixed. For WSC, we additionally allow for systematic variations in the number density from variations in the zeropoint between SuperCOSMOS plates. We add a template to the model

⁴ The details of both these catalogs can be found in [41] and [42].

⁵ The details for the construction of the mask are mentioned in the Appendix.

$C_\ell^{\text{plate}} = A \exp[-2(\ell\theta_{\text{plate}})^2/12]$, where θ_{plate} is the plate scale, 5° [63]. Finally, we fix the shot noise to the inverse of the angular number density (in steradians) except for the $0.4 < z < 0.5$ bin, where we adjust it downwards by 5% to match the high- ℓ power of C_ℓ^{gg} . For the other bins, we check that $1/\bar{n}_g$ matches the high- ℓ power in C_ℓ^{gg} , and the discrepancies are small compared to the clustering amplitude at $10 < \ell < 40$.

To model the redshift distribution, we convolve the observed photometric redshift distribution with a Gaussian for 2MPZ [64] and a generalized Lorentzian for WSC, $P(\delta z) \propto \left(1 + \frac{\delta z^2}{2as^2}\right)^{-a}$ [65]. The width evolves as a function of redshift, for the Gaussian following $\sigma = 0.027 \tanh(-20.78z_p^2 + 7.76z_p + 0.05)/(1 + z_p)$, i.e. increasing from 0.0013 at $z_p = 0$ to 0.013 at $z_p = 0.1$; and for the Lorentzian, $a(z_c) = -4z_c + 3$ and $s(z_c) = 0.04z_c + 0.02$, where z_c is the midpoint of each redshift bin. Other choices for the redshift error (e.g. redshift-independent modified Lorentzian for 2MPZ in [41] and [65]) yield very similar results.

We then use the inferred galaxy auto power spectrum to model the cross-power spectrum between the GW sources and galaxy as $C_\ell^{gwg}(z) = b_{gw}(z)/b_g(z)C_\ell^{gg}(z)$. On the GW side, we construct three GW maps from the selected GW samples composed of Set-1 (GW190814), Set-2 (GW170818, GW1901412, GW190720.000836, GW2001129.065458, GW200311.115853), and Set-3 (GW190701.203306, GW200224.222234). These maps are constructed on the basis of their luminosity distance distribution. Sources with a similar maximum value of the posterior distribution are combined to enhance the cross-correlation signal. However, due to fewer sources, the shot noise for GW sources is very large compared to the galaxies (by nearly 4-6 orders of magnitude depending on the redshift bin). So, the GW auto-correlation signal is completely dominated by shot noise.

The joint estimation of the Hubble constant along with the matter density and GW bias parameters are shown in Fig. 4. Constraints on the Hubble constant are bimodal, with the median value $H_0 = 68.2_{-6.2}^{+26.0}$ km/s/Mpc (the upper and the lower limit indicates the 68.3% equal-tailed interval (ETI)). At the lower end of the H_0 constraints, the constraints arise from the absence of the angular cross-correlation signal between the GW sources and the galaxies in the first z -bin. Due to the limited number of GW sources, we are not able to detect the cross-correlation signal with galaxies (see Fig. 6 in the appendix for further details.). The parameter constraints are driven by the structure in the cross-correlation signal and its covariance for different redshifts. Also, there are few galaxies at high redshift and the galaxy clustering signal is shot noise-dominated there. As a result, the galaxy-GW source cross-correlation does not add any additional information at high redshift. This leads to weak constraints at high H_0 and is one of the major sources of

uncertainty. Particularly for Set-3, the constraints at the high $H_0 > 90$ km/s/Mpc are affected due unavailability of catalog above $z = 0.5$. Along with this, the uncertainties on the galaxies' photometric redshifts and GW luminosity distance, and the limited number of sources, play a crucial role in the weak constraints. The value of the matter density Ω_m and bias parameter $b_{GW}(z)$ are not constrained. The estimated parameters obtained for different values of the bin width are consistent with each other. For large choices of the ℓ -bin ($\Delta\ell \geq 10$), we are able to mitigate the effect from off-diagonal terms. The $\Delta\ell = 5$ case shows a stronger bi-modal distribution. This also implies any systematic error associated with the covariance estimation is not causing any major systematic error in the inferred value of the Hubble constant for $\Delta\ell \geq 10$.

By combining the bright standard siren measurement from GW170817 with a better measurement of peculiar velocity [66], we show the corresponding posterior on H_0 in Fig. 5 with the median value of $H_0 = 67.0_{-3.8}^{+6.3}$ km/s/Mpc (68.3% ETI). This provides tighter constraints in the value of the Hubble constant than previous measurements. In Fig. 5 we compare the GW measurements of H_0 with the measurements from Planck, $H_0 = 67.4_{-0.5}^{+0.5}$ km/s/Mpc [67] and with the measurement of $H_0 = 73.04_{-1.05}^{+1.05}$ km/s/Mpc from SH0ES [68].⁶ The current measurements from the dark sirens are not sufficiently constraining yet to resolve the tension in the value of H_0 [72, 73]. Though the systematic uncertainties in our measurement of H_0 are smaller than the statistical uncertainties, in future with more GW sources and better galaxy catalog, we will be able to better assess the influence of any systematic uncertainties.

This measurement of the expansion history does not depend directly on the choice of GW mass distribution nor on whether the mass distribution follows a power-law mass distribution or a power-law + Gaussian peak model [74]. It only depends on the maximum allowed mass of individual BHs. This is primarily because the maximum mass of the BHs determines the maximum luminosity distance up to which a source can be detected from a given detector sensitivity. This luminosity distance threshold, in combination with the allowed priors on the cosmological parameters, sets the maximum redshift in the prior on GW source redshift out to which one needs to explore the cross-correlation signal. However, with the currently existing galaxy surveys, we are not able to go beyond $z = 0.5$ due to limited sky coverage and the limited redshift reach of the galaxy catalogs.

⁶ The ACT and WMAP measurement is $H_0 = 67.6_{-1.1}^{+1.1}$ km/s/Mpc [69]. The measurement using TRGB as a calibrator is $H_0 = 69.8 \pm 0.6$ (stat) ± 1.6 (sys) [70]. The strong lensing measurement from H0LiCOW is $H_0 = 73.3_{-1.8}^{+1.7}$ km/s/Mpc [71].

The GW bias parameters encode information about the GW source population and their connection to galaxies. Hence we marginalize over the GW bias parameters to infer cosmological parameters correctly and mitigate population assumptions. At large angular scales ($\ell < 30$), the GW bias parameter is expected to follow the dark matter distribution in the linear regime, and will not exhibit scale dependence. So, in this analysis, we have not considered any scale dependence in the GW bias parameter.

Even though this is the first application of the cross-correlation technique on GW data, the measurements of H_0 presented in this work are from a low number of GW sources. As a result, the clustering of the GW sources is not measured with any statistical significance. So, the estimates of H_0 presented in this work are weak and subject to systematic uncertainties associated with small number statistics.⁷ To test the robustness of our results, we have checked the following aspects, (i) randomly varied the galaxy bias parameter within their error bars, (ii) enhanced the covariance matrix by a factor of four, (iii) changed the cosmological parameters such as $S_8 \equiv \sigma_8 \sqrt{\Omega_m}$ that is used to fit the galaxy power spectrum C_ℓ^{gg} from $S_8 = 0.832$ (Planck-2018 [75]) to a lower value $S_8 = 0.75$ as indicated by the KiDS Collaboration [76], (iv) changed the value of $H_0 = 67$ km/s/Mpc to $H_0 = 74$ km/s/Mpc [77] to estimate the galaxy bias parameters, (v) changed the galaxy sample selection by additionally removing WSC sources with a low probability of being galaxies using the SVM catalog of [78], requiring $p_{\text{gal}} > 0.67$, and (vi) changed the redshift bin width Δz to 0.05 which is comparable to the photo- z errors. The posterior on H_0 did not show any significant variation for (i)–(v) cases. For the scenario (vi), the H_0 posterior show some variation and 68.3% ETI gets bigger than the estimates presented with $\Delta z = 0.1$. This is because the galaxy redshift kernels begin to overlap due to photo- z errors, violating our assumption that the GW cross-correlations in neighboring bins are uncorrelated.

The measurement in this work agrees with the dark siren measurement of $H_0 = 67_{-12}^{+13}$ km/s/Mpc (68.3% HDI) by the LVK collaboration [35]. Though the current constraints on H_0 from LVK are driven by population assumptions, the MAP value of the distribution agrees with this measurement. This is an independent validation of the LVK population assumptions. The constraints on the higher value of H_0 from the LVK analysis arise from the empty catalog component (which is driven by the population assumption). So, the upper limit on H_0 is looser for the cross-correlation technique than for

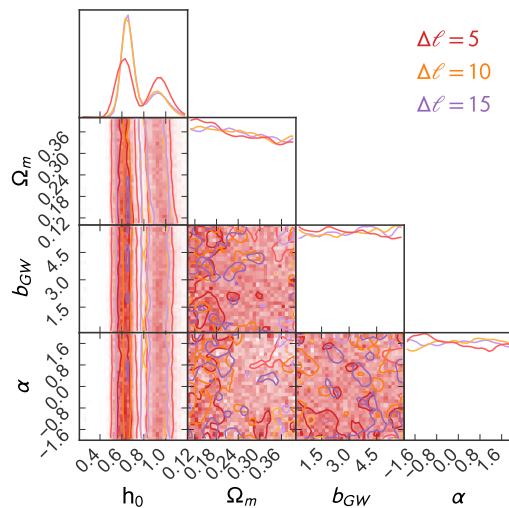


FIG. 4: The joint constraints on $H_0 = 100h_0$ km/s/Mpc, Ω_m , and $b_{GW}(z) = b_{GW}(1+z)^\alpha$ for different choices of bin-width Δl .

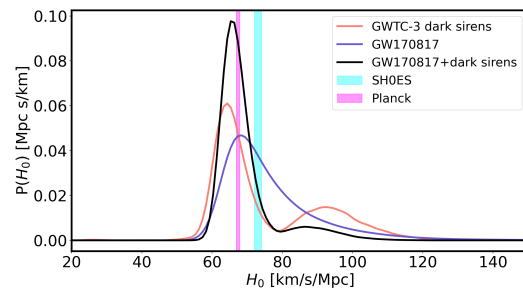


FIG. 5: Hubble constant H_0 measurement from GWTC-3 dark sirens, bright siren GW170817, and combining the both are shown along with the mean and the standard deviation on the measurements from Planck-2018 [75] and SH0ES [68].

the LVK analysis. However, at lower values of H_0 , a tighter constraint is obtained.

Conclusion and future outlook – We present the first measurement of the Hubble constant H_0 from dark standard sirens using the cross-correlation technique. The cross-correlation technique uses the spatial clustering of GW sources with galaxies and includes information beyond statistical host identification. With the best eight sources available from GWTC-3, we obtain a median value of Hubble constant $H_0 = 68.2_{-6.2}^{+26.0}$ km/s/Mpc (68.3% ETI). Due to the limited number of GW sources and absence of galaxy samples at high redshift, the cross-correlation signal is not detected, leading to only a mild improvement from the previous constraints using galaxy catalog [35]. In the future, with the availability of $z < 0.8$ spectroscopic galaxy catalogs such as DESI [79] and SPHEREx [80] (supplemented by $z > 0.8$ spectroscopy from Euclid [81] and photometric redshifts from

⁷ The measurement from other techniques such as statistical host identification and from the GW mass distribution are also affected by poor number statistics.

Vera Rubin Observatory [82]), cross-correlation of the GW sources with galaxies will be a powerful technique to measure the expansion history [12, 14, 16] and testing the general theory of relativity [15, 83].

Acknowledgements – Authors are thankful to Gergely Dalya for carefully reviewing the manuscript and providing useful comments during the LVK internal review. Authors are also thankful to Maciej Bilicki for providing insightful suggestions on the paper. Research at Perimeter Institute is supported in part by the Government of Canada through the Department of Innovation, Science and Economic Development and by the Province of Ontario through the Ministry of Colleges and Universities. SM is supported by the Simons Foundation. AK thanks the AMTD Foundation for support. This analysis is carried out at the Symmetry computing facility of the Perimeter Institute and the Infinity cluster hosted by Institut d’Astrophysique de Paris. We thank Stephane Rouberol for smoothly running the Infinity cluster. We acknowledge the use of following packages in this work: Astropy [84, 85], emcee: The MCMC Hammer [86], Giant-Triangle-Confusogram [87], healpy[88, 89], IPython [90], Matplotlib [91], NaMaster [59], NumPy [92], and SciPy [93]. This research has made use of data obtained from the SuperCOSMOS Science Archive, prepared and hosted by the Wide Field Astronomy Unit, Institute for Astronomy, the University of Edinburgh, which is funded by the UK Science and Technology Facilities Council. The authors would like to thank the LIGO/Virgo/KAGRA scientific collaboration for providing the data. LIGO is funded by the U.S. National Science Foundation. Virgo is funded by the French Centre National de Recherche Scientifique (CNRS), the Italian Istituto Nazionale della Fisica Nucleare (INFN), and the Dutch Nikhef, with contributions by Polish and Hungarian institutes. This material is based upon work supported by NSF’s LIGO Laboratory which is a major facility fully funded by the National Science Foundation.

* smukherjee1@perimeterinstitute.ca

† akrolews@uwaterloo.ca

‡ wandelt@iap.fr

§ joseph.silk@physics.ox.ac.uk, silk@iap.fr

- [1] B. P. Abbott, R. Abbott, T. D. Abbott, M. R. Abernathy, F. Acernese, K. Ackley, C. Adams, T. Adams, P. Addesso, R. X. Adhikari, et al. (LIGO Scientific Collaboration and Virgo Collaboration), *Phys. Rev. Lett.* **116**, 061102 (2016), .
- [2] J. Aasi et al. (LIGO Scientific), *Class. Quant. Grav.* **32**, 074001 (2015), 1411.4547.
- [3] B. P. Abbott et al., *Phys. Rev. D* **93**, 112004 (2016), [Addendum: *Phys.Rev.D* 97, 059901 (2018)], 1604.00439.
- [4] F. Acernese, M. Agathos, K. Agatsuma, D. Aisa, N. Allemandou, A. Allocca, J. Amarni, P. Astone, G. Balestri, G. Ballardin, et al., *Classical and Quantum Gravity* **32**, 024001 (2014), ISSN 1361-6382, .
- [5] F. Acernese, M. Agathos, L. Aiello, A. Allocca, A. Amato, S. Ansoldi, S. Antier, M. Arène, N. Arnaud, S. Ascenzi, et al. (Virgo Collaboration), *Phys. Rev. Lett.* **123**, 231108 (2019), .
- [6] T. Akutsu et al. (KAGRA), *Nat. Astron.* **3**, 35 (2019), 1811.08079.
- [7] T. Akutsu et al. (KAGRA), arXiv:2005.05574 (2020), 2005.05574.
- [8] B. F. Schutz, *Nature* **323**, 310 (1986).
- [9] M. Oguri, *Phys. Rev. D* **93**, 083511 (2016), .
- [10] S. Bera, D. Rana, S. More, and S. Bose, *Astrophys. J.* **902**, 79 (2020), 2007.04271.
- [11] G. Cañas-Herrera, O. Contigiani, and V. Vardanyan, *ApJ* **918**, 20 (2021), 2105.04262.
- [12] S. Mukherjee and B. D. Wandelt, arXiv:1808.06615 (2018), 1808.06615.
- [13] S. Mukherjee, B. D. Wandelt, and J. Silk, *Mon. Not. Roy. Astron. Soc.* **494**, 1956 (2020), 1908.08951.
- [14] S. Mukherjee, B. D. Wandelt, S. M. Nissanke, and A. Silvestri, *Phys. Rev. D* **103**, 043520 (2021), 2007.02943.
- [15] S. Mukherjee, B. D. Wandelt, and J. Silk, *Mon. Not. Roy. Astron. Soc.* **502**, 1136 (2021), 2012.15316.
- [16] C. Cigarrón Díaz and S. Mukherjee, *MNRAS* **511**, 2782 (2022), 2107.12787.
- [17] C. L. MacLeod and C. J. Hogan, *Phys. Rev. D* **77**, 043512 (2008), 0712.0618.
- [18] W. Del Pozzo, *Phys. Rev. D* **86**, 043011 (2012), 1108.1317.
- [19] M. Arabsalmani, V. Sahní, and T. D. Saini, *Phys. Rev. D* **87**, 083001 (2013), 1301.5779.
- [20] H.-Y. Chen, M. Fishbach, and D. E. Holz, *Nature* **562**, 545 (2018), 1712.06531.
- [21] R. Gray, I. M. n. Hernandez, H. Qi, A. Sur, P. R. Brady, H.-Y. Chen, W. M. Farr, M. Fishbach, J. R. Gair, A. Ghosh, et al., *Phys. Rev. D* **101**, 122001 (2020), .
- [22] M. Fishbach et al. (LIGO Scientific, Virgo), *Astrophys. J. Lett.* **871**, L13 (2019), 1807.05667.
- [23] B. Abbott et al. (LIGO Scientific, Virgo), arXiv:1908.06060 (2019), 1908.06060.
- [24] M. Soares-Santos et al. (DES, LIGO Scientific, Virgo), *Astrophys. J. Lett.* **876**, L7 (2019), 1901.01540.
- [25] R. Abbott et al. (LIGO Scientific, Virgo), *Astrophys. J.* **896**, L44 (2020), 2006.12611.
- [26] S. Borhanian, A. Dhani, A. Gupta, K. Arun, and B. Sathyaprakash (2020), 2007.02883.
- [27] S. R. Taylor, J. R. Gair, and I. Mandel, *Phys. Rev. D* **85**, 023535 (2012), 1108.5161.
- [28] W. M. Farr, M. Fishbach, J. Ye, and D. Holz, *Astrophys. J. Lett.* **883**, L42 (2019), 1908.09084.
- [29] S. Mastroianni, K. Leyde, C. Karathanasis, E. Chassande-Mottin, D. A. Steer, J. Gair, A. Ghosh, R. Gray, S. Mukherjee, and S. Rinaldi, arXiv:2103.14663 (2021), 2103.14663.
- [30] Z.-Q. You, X.-J. Zhu, G. Ashton, E. Thrane, and Z.-H. Zhu, *Astrophys. J.* **908**, 215 (2021), 2004.00036.
- [31] M. Mancarella, E. Genoud-Prachex, and M. Maggiore (2021), 2112.05728.
- [32] S. Mukherjee (2021), 2112.10256.
- [33] K. Leyde, S. Mastroianni, D. A. Steer, E. Chassande-Mottin, and C. Karathanasis (2022), 2202.00025.
- [34] J. M. Ezquiaga and D. E. Holz (2022), 2202.08240.
- [35] R. Abbott et al. (LIGO Scientific, VIRGO, KAGRA) (2021), 2111.03604.

- [36] G. Dályá, G. Galgóczi, L. Dobos, Z. Frei, I. S. Heng, R. Macas, C. Messenger, P. Raffai, and R. S. de Souza, *Mon. Not. Roy. Astron. Soc.* **479**, 2374 (2018), 1804.05709.
- [37] G. Dályá et al. (2021), 2110.06184.
- [38] A. Finke, S. Foffa, F. Iacovelli, M. Maggiore, and M. Mancarella, arXiv:2101.12660 (2021), 2101.12660.
- [39] A. Palmese, C. R. Bom, S. Mucesh, and W. G. Hartley (2021), 2111.06445.
- [40] R. Abbott et al. (LIGO Scientific, VIRGO, KAGRA) (2021), 2111.03606.
- [41] M. Bilicki, T. H. Jarrett, J. A. Peacock, M. E. Cluver, and L. Steward, *Astrophys. J. Suppl.* **210**, 9 (2014), 1311.5246.
- [42] M. Bilicki et al., *Astrophys. J. Suppl.* **225**, 5 (2016), 1607.01182.
- [43] R. Zhou et al., *Mon. Not. Roy. Astron. Soc.* **501**, 3309 (2021), 2001.06018.
- [44] J. A. Newman, *Astrophys. J.* **684**, 88 (2008), 0805.1409.
- [45] B. Menard, R. Scranton, S. Schmidt, C. Morrison, D. Jeong, T. Budavari, and M. Rahman, arXiv:1303.4722 (2013), 1303.4722.
- [46] S. Schmidt, B. Menard, R. Scranton, C. Morrison, and C. McBride, *Mon. Not. Roy. Astron. Soc.* **431**, 3307 (2013), 1303.0292.
- [47] T. H. Jarrett, T. Chester, R. Cutri, S. Schneider, M. Skrutskie, and J. P. Huchra, *AJ* **119**, 2498 (2000), astro-ph/0004318.
- [48] M. F. Skrutskie, R. M. Cutri, R. Stiening, M. D. Weinberg, S. Schneider, J. M. Carpenter, C. Beichman, R. Capps, T. Chester, J. Elias, et al., *AJ* **131**, 1163 (2006).
- [49] E. L. Wright, P. R. M. Eisenhardt, A. K. Mainzer, M. E. Ressler, R. M. Cutri, T. Jarrett, J. D. Kirkpatrick, D. Padgett, R. S. McMillan, M. Skrutskie, et al., *AJ* **140**, 1868 (2010), 1008.0031.
- [50] N. C. Hambly, H. T. MacGillivray, M. A. Read, S. B. Tritton, E. B. Thomson, B. D. Kelly, D. H. Morgan, R. E. Smith, S. P. Driver, J. Williamson, et al., *MNRAS* **326**, 1279 (2001), astro-ph/0108286.
- [51] N. C. Hambly, M. J. Irwin, and H. T. MacGillivray, *MNRAS* **326**, 1295 (2001), astro-ph/0108290.
- [52] N. C. Hambly, A. C. Davenhall, M. J. Irwin, and H. T. MacGillivray, *MNRAS* **326**, 1315 (2001), astro-ph/0108291.
- [53] J. A. Peacock, N. C. Hambly, M. Bilicki, H. T. MacGillivray, L. Miller, M. A. Read, and S. B. Tritton, *MNRAS* **462**, 2085 (2016), 1607.01189.
- [54] H. S. Xavier, M. V. Costa-Duarte, A. Balaguera-Antolínez, and M. Bilicki, *JCAP* **2019**, 037 (2019), 1812.08182.
- [55] A. Krolewski et al., *Under preparation* (2022–).
- [56] A. A. Collister and O. Lahav, *PASP* **116**, 345 (2004), astro-ph/0311058.
- [57] R. Takahashi, M. Sato, T. Nishimichi, A. Taruya, and M. Oguri, *ApJ* **761**, 152 (2012), 1208.2701.
- [58] E. Hivon, K. M. Górski, C. B. Netterfield, B. P. Crill, S. Prunet, and F. Hansen, *ApJ* **567**, 2 (2002), astro-ph/0105302.
- [59] D. Alonso, J. Sanchez, and A. Slosar (LSST Dark Energy Science), *Mon. Not. Roy. Astron. Soc.* **484**, 4127 (2019), 1809.09603.
- [60] J. Grain, M. Tristram, and R. Stompor, *Phys.Rev.D* **79**, 123515 (2009), 0903.2350.
- [61] D. J. Schlegel, D. P. Finkbeiner, and M. Davis, *ApJ* **500**, 525 (1998), astro-ph/9710327.
- [62] A. G. A. Brown, A. Vallenari, T. Prusti, J. H. de Bruijne, F. Mignard, R. Drimmel, C. Babusiaux, C. A. Bailer-Jones, U. Bastian, M. Biermann, et al., *Astronomy & Astrophysics* **595**, A2 (2016), ISSN 1432-0746, .
- [63] N. Koukoufilippas, D. Alonso, M. Bilicki, and J. A. Peacock, *MNRAS* **491**, 5464 (2020), 1909.09102.
- [64] A. Balaguera-Antolínez, M. Bilicki, E. Branchini, and A. Postiglione, *MNRAS* **476**, 1050 (2018), 1711.04583.
- [65] J. A. Peacock and M. Bilicki, *MNRAS* **481**, 1133 (2018), 1805.11525.
- [66] S. Mukherjee, G. Lavaux, F. R. Bouchet, J. Jasche, B. D. Wandelt, S. M. Nissanke, F. Leclercq, and K. Hotokezaka, *Astron. Astrophys.* **646**, A65 (2021), 1909.08627.
- [67] N. Aghanim et al. (Planck), *Astron. Astrophys.* **641**, A6 (2020), [Erratum: *Astron.Astrophys.* 652, C4 (2021)], 1807.06209.
- [68] A. G. Riess et al. (2021), 2112.04510.
- [69] S. Aiola et al. (ACT), *JCAP* **12**, 047 (2020), 2007.07288.
- [70] W. L. Freedman, *Astrophys. J.* **919**, 16 (2021), 2106.15656.
- [71] K. C. Wong et al., *Mon. Not. Roy. Astron. Soc.* **498**, 1420 (2020), 1907.04869.
- [72] L. Verde, T. Treu, and A. Riess, in *Tensions between the Early and the Late Universe* (2019), 1907.10625.
- [73] E. Di Valentino, O. Mena, S. Pan, L. Visinelli, W. Yang, A. Melchiorri, D. F. Mota, A. G. Riess, and J. Silk, *Class. Quant. Grav.* **38**, 153001 (2021), 2103.01183.
- [74] R. Abbott et al. (LIGO Scientific, VIRGO, KAGRA) (2021), 2111.03634.
- [75] N. Aghanim et al. (Planck), arXiv: 1807.06209 (2018), 1807.06209.
- [76] C. Heymans, T. Tröster, M. Asgari, C. Blake, H. Hildebrandt, B. Joachimi, K. Kuijken, C.-A. Lin, A. G. Sánchez, J. L. van den Busch, et al., *A&A* **646**, A140 (2021), 2007.15632.
- [77] A. G. Riess, S. Casertano, W. Yuan, L. M. Macri, and D. Scolnic, *Astrophys. J.* **876**, 85 (2019), 1903.07603.
- [78] T. Krakowski, K. Małek, M. Bilicki, A. Pollo, A. Kurcz, and M. Krupa, *A&A* **596**, A39 (2016), 1607.01188.
- [79] A. Aghamousa et al. (DESI) (2016), 1611.00036.
- [80] O. Dore et al., arXiv (2018), 1805.05489.
- [81] A. Blanchard et al. (Euclid), *Astron. Astrophys.* **642**, A191 (2020), 1910.09273.
- [82] LSST Science Collaboration, P. A. Abell, J. Allison, S. F. Anderson, J. R. Andrew, J. R. P. Angel, L. Armus, D. Arnett, S. J. Asztalos, T. S. Axelrod, et al., *ArXiv e-prints* (2009), 0912.0201.
- [83] S. Mukherjee, A. Krolewski, et al., *Under preparation* (2022–).
- [84] Astropy Collaboration, T. P. Robitaille, E. J. Tollerud, P. Greenfield, M. Droettboom, E. Bray, T. Aldcroft, M. Davis, A. Ginsburg, A. M. Price-Whelan, et al., *A&A* **558**, A33 (2013), 1307.6212.
- [85] Astropy Collaboration, A. M. Price-Whelan, B. M. Sipőcz, H. M. Günther, P. L. Lim, S. M. Crawford, S. Conseil, D. L. Shupe, M. W. Craig, N. Dencheva, et al., *AJ* **156**, 123 (2018), 1801.02634.
- [86] D. Foreman-Mackey, D. W. Hogg, D. Lang, and J. Goodman, *PASP* **125**, 306 (2013), 1202.3665.
- [87] S. Bocquet and F. W. Carter, *The Journal of Open Source Software* **1** (2016), .

- [88] K. M. Górski, E. Hivon, A. J. Banday, B. D. Wandelt, F. K. Hansen, M. Reinecke, and M. Bartelman, *Astrophys. J.* **622**, 759 (2005), astro-ph/0409513.
- [89] A. Zonca, L. Singer, D. Lenz, M. Reinecke, C. Rosset, E. Hivon, and K. Gorski, *Journal of Open Source Software* **4**, 1298 (2019), .
- [90] F. Pérez and B. E. Granger, *Computing in Science and Engineering* **9**, 21 (2007), ISSN 1521-9615, .
- [91] J. D. Hunter, *Computing In Science & Engineering* **9**, 90 (2007).
- [92] S. van der Walt, S. C. Colbert, and G. Varoquaux, *Computing in Science and Engineering* **13**, 22 (2011), 1102.1523.
- [93] E. Jones, T. Oliphant, P. Peterson, et al., *SciPy: Open source scientific tools for Python* (2001–), [Online; accessed [today](#)], .
- [94] D. Alonso, A. I. Salvador, F. J. Sánchez, M. Bilicki, J. García-Bellido, and E. Sánchez, *MNRAS* **449**, 670 (2015), 1412.5151.
- [95] M. Rafei-Ravandi, K. M. Smith, D. Li, K. W. Masui, A. Josephy, M. Dobbs, D. Lang, M. Bhardwaj, C. Patel, K. Bandura, et al., *ApJ* **922**, 42 (2021), 2106.04354.
- [96] A. Krolewski, S. Ferraro, E. F. Schlafly, and M. White, *JCAP* **2020**, 047 (2020), 1909.07412.
- [97] C. P. Novaes, A. Bernui, H. S. Xavier, and G. A. Marques, *MNRAS* **478**, 3253 (2018), 1805.04078.

Cross-correlation signal between GW sources and galaxies

The cross-correlation between the GW sources and galaxies are dominated by poor number statistics and we do not measure any cross-correlation clustering signal with statistical significance. We show the measured band average cross-correlation signal \hat{C}_ℓ^{GWg} as a function of redshift in Fig. 6 for $\Delta\ell = 15$ with the three GW maps constructed from the eight events. The value of maximum multipole $\ell_{\max} = 30$ is chosen to take into account the poor sky localization error of the GW sources for sources with sky localization error $\Delta\Omega \leq 30$ sq. deg. The diagonal error bars are shown on the measured values. The band average signal shows a signal that is consistent with zero at all the redshift bins. The constraints on the clustering signal at low redshift z for all the three cases drives the constraints on the lower value of $H_0 \leq 50$ km/s/Mpc. For the higher redshift bins, a non-zero mean value causes a non-zero posterior distribution on H_0 which is different from the prior (taken as $\mathcal{U}[20, 120]$ km/s/Mpc. This indicates that the constraints are weak and are affected by the systematic associated with the non-detection of the cross-correlation signal. At high redshift ($z > 0.5$) the absence of sufficient galaxies leads to an abrupt cut in the galaxy distribution and provides no information on higher values of H_0 . Due to the absence of detection of the clustering signal, the statistical power of measuring H_0 is similar to the statistical host identification technique.

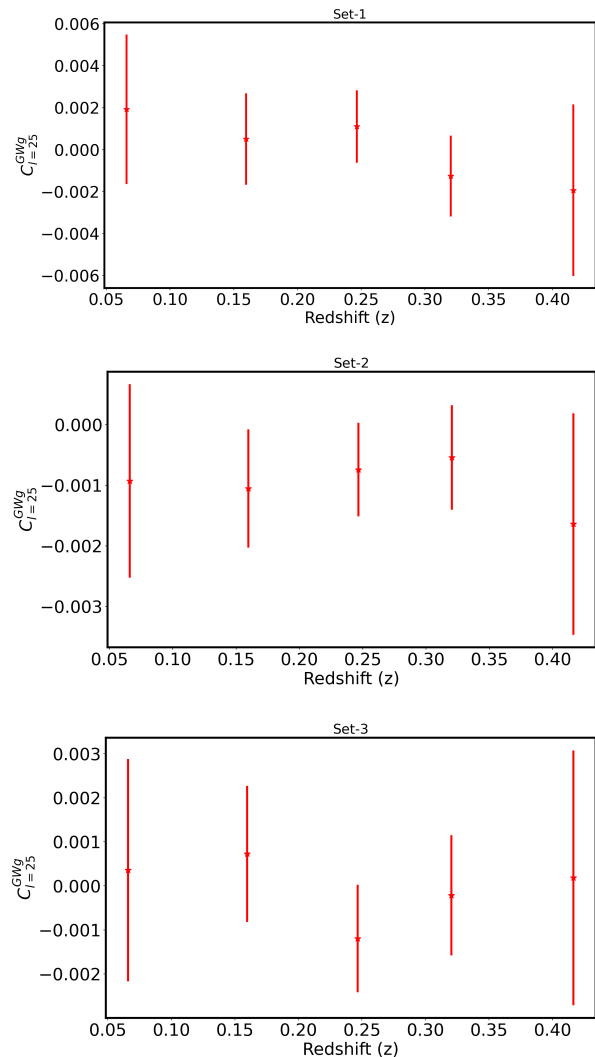


FIG. 6: The band average cross-correlation power spectrum between GW sources and galaxies with a $\Delta\ell = 15$ bin-width is shown for three different maps of the GW sources Set-1 (GW190814), Set-2 (GW170818, GW1901412, GW190720_000836, GW2001129_065458, GW200311_115853), and Set-3 (GW190701_203306, GW200224_222234) composed from the selected eight events, as a function of the median value of the redshift bin.

Construction of galaxy mask for 2MPZ and WSC

The galaxy masks were carefully constructed to remove areas with large numbers of stars or other systematics that could affect galaxy clustering, either by direct stellar contamination or by correlations, e.g. suppressed galaxy density in regions of high stellar density or extinction. We follow [64] to construct the 2MPZ mask, starting by masking low Galactic latitudes ($|b| < 10^\circ$, areas of high galactic extinction ($E(B - V) > 0.3$ from [61], and areas of high stellar density as estimated from the 2MASS

Point Source Catalog ($\log n_{\text{star}} > 3.5$)⁸. We further include manual cutouts around the LMC and SMC, excluding $275.47 < \text{RA} < 285.47$ and $-37.89 < \text{DEC} < -27.89$, and $300.81 < \text{RA} < 304.81$ and $-46.33 < \text{DEC} < -42.33$. Finally, we mask additional areas with low completeness in 2MPZ, determined by comparing the number counts of 2MPZ sources and 2MASS XSC sources (with $K_s < 13.9$) in NSIDE=64 HEALPixes. We remove pixels with $< 85\%$ completeness, mostly corresponding to areas of lower depth around bright stars. We test variations in the masking procedure (i.e. additionally multiplying by the WSC mask, following [94], or changing the completeness threshold to 80% or 90%) and find minimal changes in results.

For WSC, we follow the masking procedure of [54]. We start with the mask distributed with the WSC data release [42]⁹. We additionally mask regions with high extinction ($E(B-V) > 0.10$) and high stellar density (density of stars from GAIA greater than 7 times the mean). We additionally test several variations in the masking procedure, adding an additional mask at low Galactic latitudes following [95]; adding a WISE bright stars mask

[96]; and adding a mask of regions in WISE with high moon contamination, as determined by HEALPix pixels in which GLADE+ [37] is incomplete compared to WSC. We also test variations in the sample-selection procedure, i.e. additionally using the SVM catalog of [78] to restrict to likely galaxies [95, 97]. We find that these variations generally lead to a scale-independent shift in the amplitude of C_ℓ^{gg} , either corresponding to a change in galaxy bias due to differing populations, or a change in the stellar contamination fraction, which is entirely degenerate with bias at $\ell > 10$ where the stellar power spectrum is small. In this regime, the effect of changing stellar contamination is degenerate with bias in both the galaxy auto spectrum and the galaxy cross-spectrum with GW sources, so it will cause systematic errors in our modeling.

We assume that the galaxy bias is redshift-independent in each bin, and obtain best-fit values of $b_g(z_c = 0.05) = 1.18$, $b_g(z_c = 0.15) = 0.66$, $b_g(z_c = 0.25) = 1.35$, $b_g(z_c = 0.35) = 1.76$, and $b_g(z_c = 0.45) = 2.33$. The very low value of b_g in the second bin is driven by the SuperCOSMOS plate template, which is degenerate with the cosmological contribution due to the limited multipole range considered ($10 < \ell < 40$).

⁸ <https://www.ipac.caltech.edu/2mass/releases/allsky/doc/sec4.5c.html>